# Theoretical Approach Using DFT Calculations of Novel Oxime Derivatives

**Siyamak Shahab** [1,2,3]**, Masoome Sheikhi** [4]**, Khadijeh Shekoohi** [5]**, Sadegh Kaviani** [6]**, Abolfazl Shiroudi** [7]**, Elham Zarenezhad** [8,*] 

[1]   Belarussian State University, ISEI BSU, Minsk, Republic of Belarus
[2]   Institute of Physical Organic Chemistry, National Academy of Sciences of Belarus, 13 Surganov Str., Minsk 220072
[3]   Institute of Chemistry of New Materials, National Academy of Sciences of Belarus, 36 Skarina Str., Minsk 220141
[4]   Young Researchers and Elite Club, Gorgan Branch, Islamic Azad University, Gorgan, Iran
[5]   Department of Chemistry, Darab Branch, Islamic Azad University, Darab 7481783143-196, Iran
[6]   Department of Chemistry, Ferdowsi University of Mashhad, Mashhad, Iran
[7]   Young Researchers and Elite Club, East Tehran Branch, Islamic Azad University, Tehran, Iran
[8]   Noncommunicable Diseases Research Center, Fasa University of Medical Sciences, Fasa, Iran
*   Correspondence: El.zarenezhad@gmail.com, El.zarenezhad@fums.ac.ir  (E.Z.);

**Abstract:** This study used the density functional theory (DFT) methods to evaluate the geometrical properties, UV, the lowest unoccupied molecular orbital (LUMO), the highest occupied molecular orbital (HOMO) analysis, and the molecular electrostatic potential (MEP) of oxime ether derivatives containing a quinoxaline. In addition, the stability of the molecule resulting from hyper conjugative interactions charge delocalization was studied using a natural bond orbital (NBO) analysis. The HOMO-LUMO energy gaps indicated different charge-transfer possibilities within the regarded molecules. Eventually, NBO analysis demonstrates the charge transfer between the lone pairs and the localized bonds.

## 1. Introduction

Synthesis of novel biologically active heterocyclic compounds is undertaken with the ultimate hope of the development of drugs [1]. Heterocyclic compounds containing nitrogen heteroatoms have recently attracted attention due to their considerable potential as pharmacotherapeutic agents [2]. The presence of a heterocyclic nitrogen nucleus in the framework of various pharmacologically active compounds representing antibacterial, antiasthmatic, antitumor, antimalarial, antileishmanial, antiplatelet, and anthelmintic properties justifies their synthesis [3, 4]. Quinoxalines are important classes of nitrogen-containing heterocyclic compounds which have shown a wide variety of applications in pharmacology, so they have received special interest from synthetic chemists for many years. These invaluable heterocycles have shown different pharmacological activities [5]. Previously our group synthesized quinoxaline derivatives with good bactericide activity [6].

DFT methods have been widely used to verify experimental measurements for biological systems [7]. Several experimental and molecular modeling studies have been reported on the electronic structure of quinoxalines derivatives [8−11]. At the same time, there are not many theoretical studies on their electronic structures, quantum descriptors, and

biological activities of them. Behzadi and coworkers studied the correlation between electronic parameters and the biological activity of some quinoxaline derivatives [12]. They concluded that the activity of corresponding drugs increases with the increasing electron-withdrawing property of the molecule. In another study, Hebat-Allah and coworkers reported molecular modeling and synthesizing some quinoxaline derivatives as anticancer drugs [13]. Based on their research, these compounds show more inhibition activity of C-met kinase than doxorubicin. Corona et al. [14] synthesized a series of quinoxaline compounds to test their antitumor activity for different types of human cancers. The findings showed that benzyl amino quinoxaline derivatives have the most antitumor activity. Due to the importance of quinoxalines as an N-heterocyclic compound in therapeutic medicine, continuing the existing interest in the design and synthesis of new N-heterocyclic compounds [15–17], the present study explains the design of new quinoxaline derivatives and the DFT studies of their new derivatives.

## 2. Materials and Methods

The quantum chemical calculations of molecules **1a**, **1b**, **1c**, **1d**, and **1e** were carried out using Gaussian 09 software programs [18].optimizing the molecular structure of studied molecules was done by the DFT method (functional PBE1PBE) along with the 6-31+G$^*$ basis set [18] in solvent water. To quantify the solvent effect, the polarized continuum model (PCM) [19] was used. Without any geometry constraint, the energies of the molecules described above have been minimized; all intramolecular forces have been taken to zero.

Using the EHOMO and ELUMO energies at the PBE1PBE/6-31+G$^*$ level, we obtained HOMO-LUMO energy gap (Eg), electron affinity, global hardness, ionization potential, electronic chemical potential, electrophilicity, electronegativity, and chemical softness. To study the electronic transitions of new molecules, we have used the TD-DFT method [20]. The theoretical absorption spectra of the studied molecules in solvent water were determined using the TDPBE1PBE/6-31+G$^*$ method. We visualized optimized molecular structures, HOMO-LUMO gaps, molecular electrostatic potential (MEP) maps, and UV spectra by using the GaussView program [21]. The electronic structure of molecule 5d was investigated using natural bond orbital (NBO) analysis [22]. Finally, hyper conjugative interactions and charge delocalization are measured at the PBE1PBE/6-31+G$^*$ level of theory.

## 3. Results and Discussion

The structure of some novel oxime ether derivatives containing a quinoxaline moiety is shown in Scheme 1.
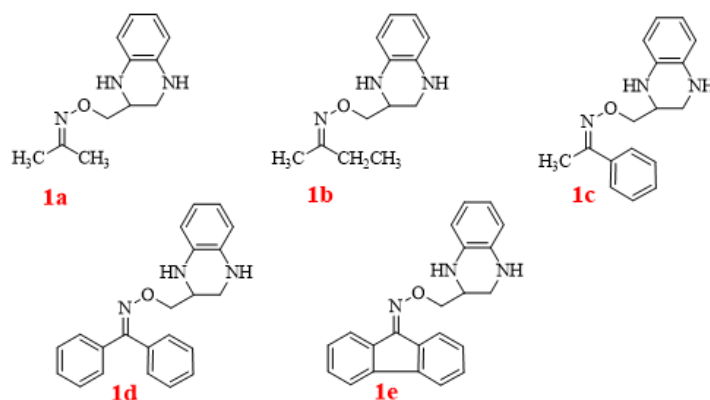


**Scheme 1**. Structure of some novel oxime ether derivatives containing a quinoxaline moiety.

The optimized structures of all the considered compounds were studied by a comprehensive computational method, namely PBE1PBE/6-31+G$^*$ theoretical level discussed in this work.

### 3.1. Frontier molecule orbitals analysis.

As can be seen in Figure 1, the optimized molecular structures of compounds 1a−e were shown. LUMO and HOMO are known as the frontier molecule orbitals (FMOs), which participate in optical properties, UV spectrum, chemical reactions, and electronic properties [20, 23]. We have calculated the HOMO–LUMO orbital energy and electronic properties of compounds 1a-e using PBE1PBE/6-31+G$^*$ theoretical level and summarized in Table 1.
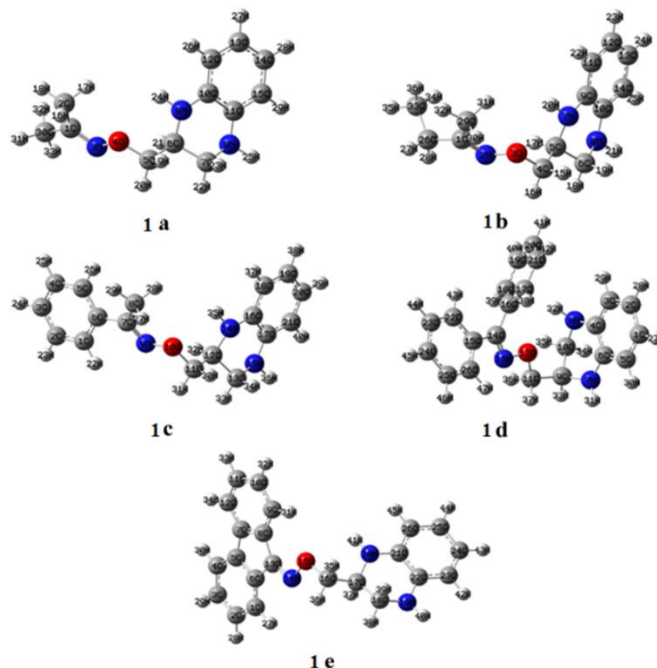


**Figure 1.** Optimized molecular structures of molecules 1a−e.

As can be seen in Figure 2, the HOMO orbitals of the molecules **1a**, **1b**, **1c**, **1d**, and **1e** are mostly based on the double bonds (−C=C−) and the nitrogen atoms of quinoxaline and oxygen atom, the LUMO orbitals of the molecules **1a**, and **1b** are localized on double bonds (−C=C−) and the nitrogen atoms of quinoxaline, while for the molecules **1c**, **1d**, and **1e** are localized on double bonds (−C=C−) of the phenyl rings and the N−O group.

**Table 1.** Calculated electronic properties of compounds **1a−e**

| Parameter | 1a | 1b | 1c | 1d | 1e |
|---|---|---|---|---|---|
| HF (Hartree) | -706.0989 | -745.3554 | -897.6045 | -1089.1015 | -1087.9341 |
| Dipole moment (Debye) | 3.3034 | 3.3887 | 3.1030 | 3.6624 | 2.8482 |
| Point Group | C1 | C1 | C1 | C1 | C1 |
| $E_{HOMO}$ (eV) | -4.30 | -4.30 | -4.32 | -4.42 | -4.35 |
| $E_{LUMO}$ (eV) | -1.09 | -1.15 | -2.16 | -2.39 | -2.97 |
| Eg (eV) | 3.21 | 3.15 | 2.16 | 2.03 | 1.38 |
| I (eV) | 4.30 | 4.30 | 4.32 | 4.42 | 4.35 |
| A (eV) | 1.09 | 1.15 | 2.16 | 2.39 | 2.97 |
| χ (eV) | 2.69 | 2.72 | 3.24 | 3.40 | 3.66 |
| η (eV) | 1.60 | 1.57 | 1.08 | 1.01 | 0.69 |
| μ (eV) | -2.69 | -2.72 | -3.24 | -3.40 | -3.66 |
| ω (eV) | 2.26 | 2.36 | 4.86 | 5.72 | 9.71 |
| S (eV) | 0.31 | 0.32 | 0.46 | 0.49 | 0.72 |

As a result, most of the charge transfer from HOMO to LUMO in the studied compounds is attributed to the contribution of lone pairs and π bonds. The negative and positive phases are in green and red colors, correspondingly. The energy gap is a significant parameter for determining the reactivity of the molecules and the properties of molecular electrical transport [24].

Molecules with a low gap have simpler electronic transport properties. The molecular system has high polarization, low kinetic stability, and high chemical reactivity; thus, the system is called a soft molecule [25]. The HOMO-LUMO energy gap values for compounds **1a**, **1b**, **1c**, **1d**, and **1e** were measured around 3.21, 3.15, 2.16, 2.18, and 1.38 eV, respectively.
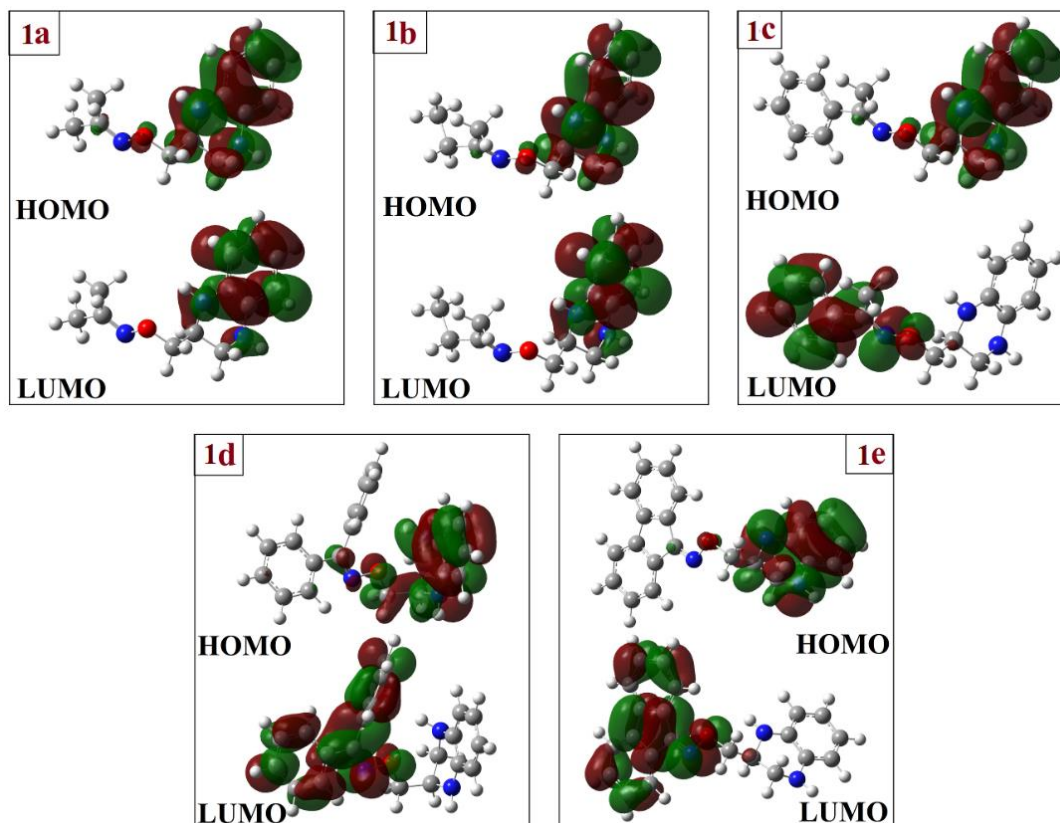


**Figure 2.** Calculated HOMO and LUMO orbitals of compounds **1a–e**.

The trend of the softness degree of the titled molecules is **1e** > **1d** > **1c** > **1b** > **1a**. The molecules are converted to a softer system by the expansion of conjugation. Also, as can be seen from Figure 3, the total electronic density of states (DOS) plots [21] show the energy gaps of the studied molecules. While molecular interactions occur, the LUMO accepts the electrons and their energy associated with the electron affinity (A), whereas the HOMO denotes electrons donors, and its energy is associated with the ionization potential (I) [24, 25]. The electronic chemical potential (μ), electronegativity (χ), global chemical hardness (η), chemical softness (S), and global electrophilicity (ω) parameters are calculated as follows [24, 26]:

$$\eta = \frac{I-A}{2} \ ; \ \chi = \frac{I+A}{2} \ ; \ \mu = -\frac{I+A}{2} \ ; \ \omega = \frac{\mu^2}{2\eta} \ ; \ S = \frac{1}{2\eta}$$

The global reactivity of the considered compounds is investigated in terms of the energy of the HOMO and LUMO and the HOMO-LUMO energy gap, which is a useful quantity for investigating kinetic stability and computed at the PBE1PBE/6-31+G$^*$ level (see Table 1). The η denotes the global chemical hardness [η =($E_{LUMO}$−$E_{HOMO}$)/2] that is associated with the

HOMO-LUMO energy gap and defined as the resistance measurement of an atom or a group of atoms to charge transfer [1−3]. A molecule with a high Eg has a low chemical reactivity and high kinetic stability because it is energetically disadvantageous to add an electron to the high-lying LUMO to remove electrons from the low-lying HOMO [3].
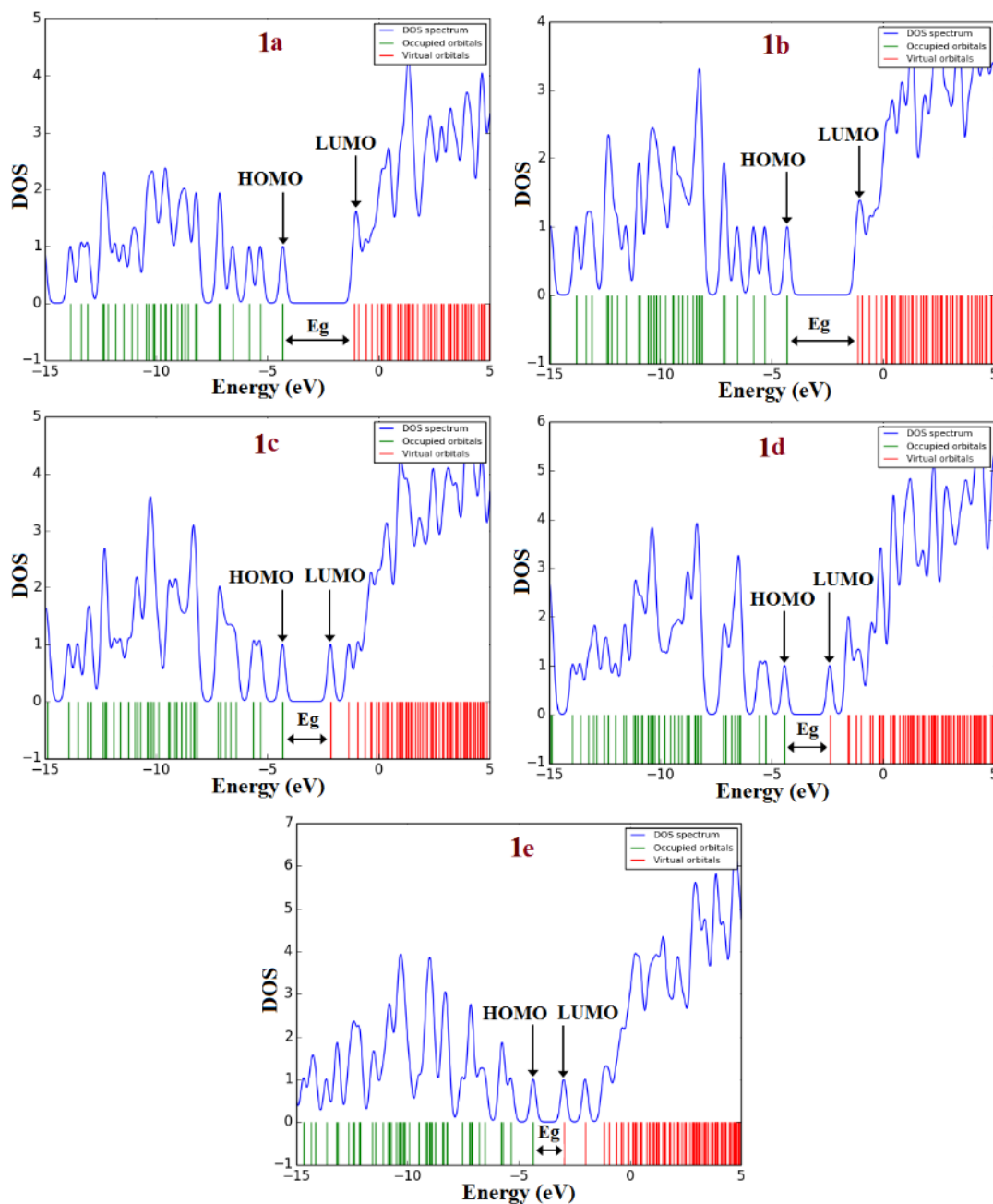


**Figure 3.** Calculated total density of states (DOS) plots of molecules **1a–e**.

The global chemical hardness values of molecules **1a**, **1b**, **1c**, **1d**, and **1e** are 1.60, 1.57, 1.08, 1.0 and 0.69 eV, respectively. The highest $\eta$ value for compound 1a is observed; thus, it's the hardest molecule relative to other molecules. The absolute electronegativity parameter is applied to investigate the electron transfer direction, which is a good measure of the molecular ability to attract electrons.
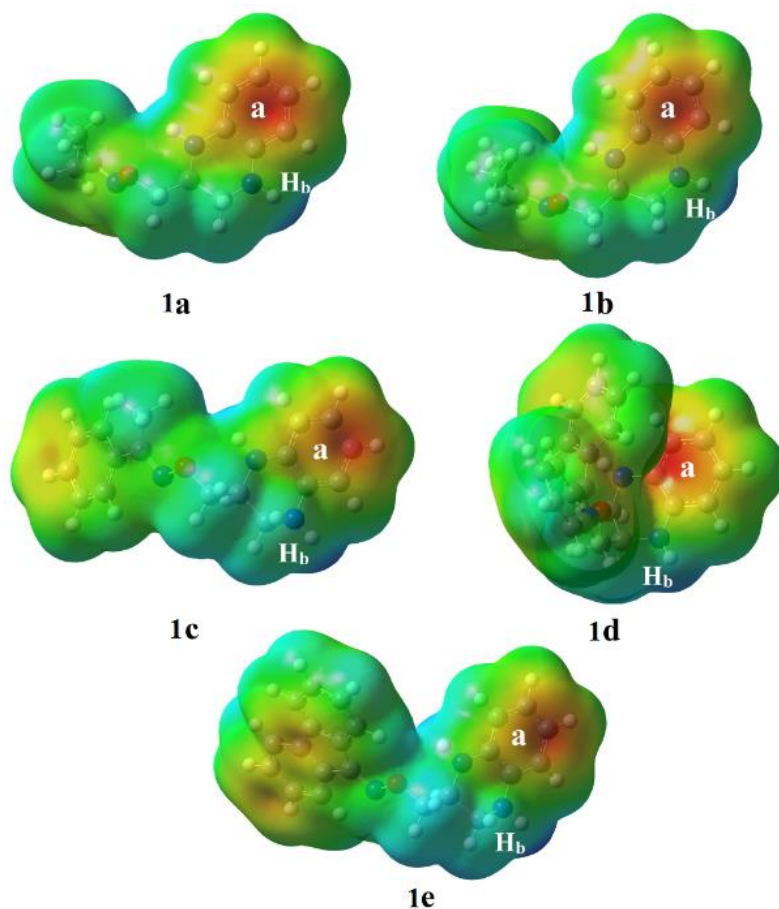
### 3.2. MEP analysis of molecules 1a−e.

MEP maps display electronic density and are used to detect positive and negative electrostatic potential regions for nucleophilic reactions and electrophilic attacks, respectively

[1, 4]. The various values of the electrostatic potential are seen in different colors, and the potential reductions are: *blue > green > yellow > orange > red.* Negative (*red*, high electron density) regions are related to the electrophilic reactivity, while the positive (*blue*, low electron density) regions are associated with the electrophilic attack sites−the molecular electrostatic potential surfaces of molecules **1a−e** are shown in Figure 4.

The negative sites of compounds **1a**, **1b**, **1c**, **1d**, and **1e** are mostly focused on the phenyl ring of quinoxaline (ring a); therefore, these sites have a high electron density and are appropriate for electrophilic attack (Figure 4). The parts of molecules **1c**, **1d**, and **1e** are pale red or orange colors that show regions with a partial negative charge, such as phenyl rings. The positive sites of the studied compounds are mostly focused on the $H_b$ of the N−H bond in quinoxaline. Furthermore, green regions show zero potential and neutral sites, like hydrogen atoms in phenyl rings and saturated C−C bonds.



**Figure 4.** The molecular electrostatic potential surface of molecules 1a−e.

### 3.3. Natural bond orbital analysis.

The natural bond orbital analysis is important for determining intra- and intermolecular interactions and defining interactions between virtual and filled orbital spaces [5]. This analysis is an important method for the chemical understanding of hyper-conjugative interactions and electron density transfer from the filled lone pair orbital of one subsystem to the empty orbital of another subsystem. The filled NBOs and empty filled NBOs and the stabilization energy, $E^{(2)}$ estimated from the 2nd order micro disturbance theory of compound **1d** are reported in Table 2. The electron delocalization from the donor orbitals to the acceptor orbitals describes a conjugative electron transfer process. For each donor NBO($i$) and acceptor NBO($j$), the

stabilization energy $E^{(2)}$ associated with electron delocalization between donor and acceptor [$i{\rightarrow}j$] is estimated as [21]:

$$E_2 = \Delta E_{ij} = q_i \left[ F_{(i,j)}^2 \Big/ (\varepsilon_i - \varepsilon_j) \right]$$

where $F_{(i,j)}$ is the off-diagonal NBO Fock matrix elements, $\varepsilon_i$ and $\varepsilon_j$ represent diagonal elements (orbital energies), and $q_i$ denotes the $i$th donor orbital occupancy.

**Table 2.** Important donor-acceptor interactions and 2nd order perturbation energies of compound **1d**.

| Donor NBO (i) | Occupancy | Acceptor NBO (j) | Occupancy | Interaction type | E(2) (kcal/mol) |
|---|---|---|---|---|---|
| $\pi_{C1-C5}$ | 1.72464 | $\pi^*_{C2-C3}$ | 0.38633 | $\pi_{C1-C5} \rightarrow \pi^*_{C2-C3}$ | 12.69 |
| | | $\pi^*_{C4-C6}$ | 0.47115 | $\pi_{C1-C5} \rightarrow \pi^*_{C4-C6}$ | 14.67 |
| $\pi_{C2-C3}$ | 1.70947 | $\pi^*_{C1-C5}$ | 0.38017 | $\pi_{C2-C3} \rightarrow \pi^*_{C1-C5}$ | 14.54 |
| | | $\pi^*_{C4-C6}$ | 0.47115 | $\pi_{C2-C3} \rightarrow \pi^*_{C4-C6}$ | 13.43 |
| $\pi_{C4-C6}$ | 1.60210 | $\pi^*_{C1-C5}$ | 0.38017 | $\pi_{C4-C6} \rightarrow \pi^*_{C1-C5}$ | 13.50 |
| | | $\pi^*_{C2-C3}$ | 0.38633 | $\pi_{C4-C6} \rightarrow \pi^*_{C2-C3}$ | 15.46 |
| $\pi_{C15-C22}$ | 1.97337 | $\pi^*_{N13-C14}$ | 0.22123 | $\pi_{C15-C22} \rightarrow \pi^*_{N13-C14}$ | 12.97 |
| | | $\pi^*_{C23-C24}$ | 0.32899 | $\pi_{C15-C22} \rightarrow \pi^*_{C23-C24}$ | 14.32 |
| | | $\pi^*_{C25-C26}$ | 0.30468 | $\pi_{C15-C22} \rightarrow \pi^*_{C25-C26}$ | 14.29 |
| $\pi_{C16-C17}$ | 1.65136 | $\pi^*_{C18-C19}$ | 0.31527 | $\pi_{C16-C17} \rightarrow \pi^*_{C18-C19}$ | 14.69 |
| | | $\pi^*_{C20-C21}$ | 0.32324 | $\pi_{C16-C17} \rightarrow \pi^*_{C20-C21}$ | 14.30 |
| $\pi_{C18-C19}$ | 1.66436 | $\pi^*_{C16-C17}$ | 0.35916 | $\pi_{C18-C19} \rightarrow \pi^*_{C16-C17}$ | 14.53 |
| | | $\pi^*_{C20-C21}$ | 0.32324 | $\pi_{C18-C19} \rightarrow \pi^*_{C20-C21}$ | 14.67 |
| $\pi^*_{N13-C14}$ | 1.93371 | $\pi^*_{C15-C22}$ | 0.37889 | $\pi^*_{N13-C14} \rightarrow \pi^*_{C15-C22}$ | 49.67 |
| | | $\pi^*_{C16-C17}$ | 0.35916 | $\pi^*_{N13-C14} \rightarrow \pi^*_{C16-C17}$ | 22.03 |
| $\sigma_{C1-C5}$ | 1.97818 | $\sigma^*_{C1-C2}$ | 0.01580 | $\sigma_{C1-C5} \rightarrow \sigma^*_{C1-C2}$ | 1.93 |
| | | $\sigma^*_{C5-C6}$ | 0.01977 | $\sigma_{C1-C5} \rightarrow \sigma^*_{C5-C6}$ | 2.29 |
| | | $\sigma^*_{C6-N7}$ | 0.02573 | $\sigma_{C1-C5} \rightarrow \sigma^*_{C6-N7}$ | 4.10 |
| $\sigma_{C3-C4}$ | 1.97440 | $\sigma^*_{C4-C6}$ | 0.03555 | $\sigma_{C3-C4} \rightarrow \sigma^*_{C4-C6}$ | 3.03 |
| | | $\sigma^*_{C4-N8}$ | 0.02446 | $\sigma_{C3-C4} \rightarrow \sigma^*_{C4-N8}$ | 1.03 |
| | | $\sigma^*_{C6-N7}$ | 0.02573 | $\sigma_{C3-C4} \rightarrow \sigma^*_{C6-N7}$ | 3.39 |
| | | $\sigma^*_{N8-C10}$ | 0.01710 | $\sigma_{C3-C4} \rightarrow \sigma^*_{N8-C10}$ | 1.99 |
| $\sigma_{C5-C6}$ | 1.97347 | $\sigma^*_{C1-C5}$ | 0.01313 | $\sigma_{C5-C6} \rightarrow \sigma^*_{C1-C5}$ | 2.01 |
| | | $\sigma^*_{C4-C6}$ | 0.03555 | $\sigma_{C5-C6} \rightarrow \sigma^*_{C4-C6}$ | 3.05 |
| | | $\sigma^*_{C4-N8}$ | 0.02446 | $\sigma_{C5-C6} \rightarrow \sigma^*_{C4-N8}$ | 3.42 |
| | | $\sigma^*_{C6-N7}$ | 0.02573 | $\sigma_{C5-C6} \rightarrow \sigma^*_{C6-N7}$ | 1.16 |
| | | $\sigma^*_{C7-C9}$ | 0.03099 | $\sigma_{C5-C6} \rightarrow \sigma^*_{C7-C9}$ | 2.35 |
| $\sigma_{O12-N13}$ | 1.98245 | $\sigma^*_{C9-C11}$ | 0.04058 | $\sigma_{O12-N13} \rightarrow \sigma^*_{C9-C11}$ | 1.16 |
| | | $\sigma^*_{C14-C15}$ | 0.03435 | $\sigma_{O12-N13} \rightarrow \sigma^*_{C14-C15}$ | 3.92 |
| $\sigma_{C14-C15}$ | 1.96061 | $\sigma^*_{O12-N13}$ | 0.03310 | $\sigma_{C14-C15} \rightarrow \sigma^*_{O12-N13}$ | 4.70 |
| | | $\sigma^*_{N13-C14}$ | 0.01947 | $\sigma_{C14-C15} \rightarrow \sigma^*_{N13-C14}$ | 1.15 |
| | | $\sigma^*_{C15-C22}$ | 0.02336 | $\sigma_{C14-C15} \rightarrow \sigma^*_{C15-C22}$ | 1.40 |
| | | $\sigma^*_{C16-C17}$ | 0.02447 | $\sigma_{C14-C15} \rightarrow \sigma^*_{C16-C17}$ | 0.81 |
| $n(1)_{N7}$ | 1.77796 | $\pi^*_{C4-C6}$ | 0.47115 | $n(1)_{N7} \rightarrow \pi^*_{C4-C6}$ | 27.97 |
| | | $\sigma^*_{C9-C10}$ | 0.04199 | $n(1)_{N7} \rightarrow \sigma^*_{C9-C10}$ | 0.59 |
| | | $\sigma^*_{C9-C11}$ | 0.04058 | $n(1)_{N7} \rightarrow \sigma^*_{C9-C11}$ | 7.96 |
| | | $\sigma^*_{C9-H33}$ | 0.01905 | $n(1)_{N7} \rightarrow \sigma^*_{C9-H33}$ | 1.85 |
| | | $\sigma^*_{C11-H36}$ | 0.02469 | $n(1)_{N7} \rightarrow \sigma^*_{C11-H36}$ | 0.61 |
| $n(1)_{N8}$ | 1.83556 | $\sigma^*_{C3-C4}$ | 0.02098 | $n(1)_{N8} \rightarrow \sigma^*_{C3-C4}$ | 0.79 |
| | | $\sigma^*_{C4-C6}$ | 0.03555 | $n(1)_{N8} \rightarrow \sigma^*_{C4-C6}$ | 3.89 |
| | | $\pi^*_{C4-C6}$ | 0.47115 | $n(1)_{N8} \rightarrow \pi^*_{C4-C6}$ | 13.35 |
| | | $\sigma^*_{C9-C10}$ | 0.04199 | $n(1)_{N8} \rightarrow \sigma^*_{C9-C10}$ | 6.70 |
| | | $\sigma^*_{C10-H34}$ | 0.01977 | $n(1)_{N8} \rightarrow \sigma^*_{C10-H34}$ | 2.56 |
| $n(1)_{O12}$ | 1.97586 | $\sigma^*_{C9-C11}$ | 0.04058 | $n(1)_{O12} \rightarrow \sigma^*_{C9-C11}$ | 0.54 |
| | | $\sigma^*_{C11-H37}$ | 0.02248 | $n(1)_{O12} \rightarrow \sigma^*_{C11-H37}$ | 1.40 |

| Donor NBO (i) | Occupancy | Acceptor NBO (j) | Occupancy | Interaction type | $E^{(2)}$ (kcal/mol) |
|---|---|---|---|---|---|
| | | $\sigma^*_{C14-C15}$ | 0.03435 | $n(1)_{O12} \rightarrow \sigma^*_{C14-C15}$ | 0.65 |
| $n(2)_{O12}$ | 184458 | $\sigma^*_{C11-H36}$ | 0.02469 | $n(2)_{O12} \rightarrow \sigma^*_{C11-H36}$ | 5.32 |
| | | $\sigma^*_{C11-H37}$ | 0.02248 | $n(2)_{O12} \rightarrow \sigma^*_{C11-H37}$ | 2.79 |
| | | $\pi^*_{N13-C14}$ | 0.22123 | $n(2)_{O12} \rightarrow \pi^*_{N13-C14}$ | 16.10 |
| $n(1)_{N13}$ | 1.94695 | $\sigma^*_{C9-C11}$ | 0.04058 | $n(1)_{N13} \rightarrow \sigma^*_{C9-C11}$ | 1.16 |
| | | $\sigma^*_{C14-C15}$ | 0.03435 | $n(1)_{N13} \rightarrow \sigma^*_{C14-C15}$ | 0.53 |
| | | $\sigma^*_{C14-C16}$ | 0.04631 | $n(1)_{N13} \rightarrow \sigma^*_{C14-C16}$ | 9.27 |

The higher value of $E^{(2)}$, the more powerful the interaction between the donor and the acceptor orbitals, *i.e.,* the greater the donation propensity of the electron donors to the electron acceptors and the greater the conjugation of the whole molecular structure. Delocalization of electron density between occupied Lewis-type (bond or lone pair) NBO orbitals and formally unoccupied (antibonding or Rydberg) non-Lewis NBO orbitals leads to the donor-acceptor stabilization relationship [4]. The NBO study was measured for molecule **1d** using the PBE1PBE/6-31+G$^*$ theoretical level to elucidate the intramolecular, rehybridization, and delocalization of electron density. The intramolecular hyper-conjugative interactions of the studied molecule with different intensity (weak, moderate, and strong) comprising $\sigma \rightarrow \sigma^*$, $\pi \rightarrow \pi^*$, $n \rightarrow \sigma^*$, $n \rightarrow \pi^*$, and $\pi^* \rightarrow \pi^*$ transitions are summarized in Table 2.

The $\sigma_{C1-C5}$ bonding orbital in the quinoxaline ring serves as a donor, and the $\sigma^*_{C1-C2}$, $\sigma^*_{C5-C6}$, and $\sigma^*_{C6-N7}$ antibonding orbitals participate as an acceptor with stabilization energy of 1.93, 2.29, and 4.1 kcal/mol, respectively. The obtained results reveal that the $\sigma_{C1-C5} \rightarrow \sigma^*_{C6-N7}$ interaction has the highest stabilization energy relative to the associated interactions.

As shown in Table 2, the intramolecular hyper-conjugative of the $\pi \rightarrow \pi^*$ interactions have the most resonance energy relative to the $\sigma \rightarrow \sigma^*$ interactions. The $\pi \rightarrow \pi^*$ interaction in the quinoxaline ring, leads to strong delocalization energy, including $\pi_{C4-C6} \rightarrow \pi^*_{C2-C3}$ with the resonance energy of 15.46 kcal/mol. The other important $\pi \rightarrow \pi^*$ interactions in the quinoxaline rings and the phenyl rings are such as $\pi_{C1-C5} \rightarrow \pi^*_{C4-C6}$, $\pi_{C2-C3} \rightarrow \pi^*_{C1-C5}$, $\pi_{C15-C22} \rightarrow \pi^*_{C23-C24}$, $\pi_{C15-C22} \rightarrow \pi^*_{C25-C26}$, $\pi_{C16-C17} \rightarrow \pi^*_{C18-C19}$, $\pi_{C16-C17} \rightarrow \pi^*_{C20-C21}$, $\pi_{C18-C19} \rightarrow \pi^*_{C16-C17}$, and $\pi_{C18-C19} \rightarrow \pi^*_{C20-C21}$, interactions with stabilization energy of 14.67, 14.54, 14.32, 14.29, 14.69, 14.30, 14.53, and 14.67 kcal/mol, respectively. The $\pi_{C15-C22}$ bonding orbital in the phenyl rings is used as a donor, and the $\pi^*_{N13-C14}$, $\pi^*_{C23-C24}$ and $\pi^*_{C25-C26}$ antibonding orbitals act as the acceptor with the stabilization energy of 12.97, 14.32 and 14.29 kcal/mol, respectively. The obtained results show that the resonance energy of $\pi_{C15-C22} \rightarrow \sigma^*_{C23-C24}$ has the highest value (14.32 kcal/mol).

The $\pi^*_{N13-C14} \rightarrow \pi^*_{C15-C22}$ interaction between N=C and phenyl ring with resonance energy of ~49.67 kcal/mol has the highest resonance energy relative to the other interactions of molecule **1d**. The interactions $n(1)_{N7} \rightarrow \pi^*_{C4-C5}$, $n(1)_{N8} \rightarrow \pi^*_{C4-C6}$, $n(2)_{O12} \rightarrow \pi^*_{N13-C14}$ with stabilization energy of 27.97, 13.35, and 16.10 kcal/mol, respectively, have the most resonance energies relative to the $n \rightarrow \sigma^*$ interactions. The interactions of $n(1)_{N13} \rightarrow \sigma^*_{C14-C16}$ have high stabilization energy of 9.27 kcal/mol relative to $n(1)_{N13} \rightarrow \sigma^*_{C9-C11}$ and $n(1)_{N13} \rightarrow \sigma^*_{C14-C15}$ with stabilization energies of 1.16 and 0.53 kcal/mol, respectively (see Table 3 and Figure 1).

The size of the polarization coefficients indicates the contribution of the two hybrids in forming bonds in the molecular system [6]. The variations in electronegativity of the atoms involved in bond-forming are reflected in the larger differences in the polarization coefficients of the atoms (C–N, C–O, and C–H bonds) [7]. The $\sigma_{C4-C6}$ bonding orbital is equal to

$\sigma=0.7046(sp^{1.90})+0.7096(sp^{1.89})$ with a high occupancy of 1.96715 a.u. and low energy of −0.62593 a.u. In the $\sigma_{C4-C6}$ bonding orbital, the polarization coefficients C4=0.7046 and C6=0.7096 suggest a low discrepancy in the polarization coefficients between the two atoms and the importance of the bond formation. The $\pi_{C1-C5}$ bonding orbital in the quinoxaline ring, measured as $\sigma=0.6973(sp^{1.00})+0.7168(sp^{1.00})$ with an occupancy of 1.72464 a.u. and the energy of −0.22076 a.u.

**Table 3.** Calculated natural bond orbital and polarization coefficient for each hybrid in chosen bonds of molecule **1d**.

| Occupancy (a.u.) | Bond (A−B)[a] | Energy (a.u.) | ED$_A$ (%) | ED$_B$ (%) | NBO | S(%) (A) | S(%) (B) | P(%) (A) | P(%) (B) |
|---|---|---|---|---|---|---|---|---|---|
| 1.97818 | $\sigma_{C1-C5}$ | −0.62134 | 49.44 | 50.56 | $0.7031\ (sp^{1.88}) + 0.7111\ (sp^{1.75})$ | 34.74 | 36.34 | 65.23 | 63.64 |
| 1.72464 | $\pi_{C1-C5}$ | −0.22076 | 48.62 | 51.38 | $0.6973\ (sp^{1.00}) + 0.7168\ (sp^{1.00})$ | 0.00 | 0.00 | 99.96 | 99.97 |
| 1.97814 | $\sigma_{C2-C3}$ | −0.61878 | 49.49 | 50.51 | $0.7035\ (sp^{1.88}) + 0.7107\ (sp^{1.77})$ | 34.66 | 36.09 | 65.31 | 63.88 |
| 1.70947 | $\pi_{C2-C3}$ | −0.21902 | 50.78 | 49.22 | $0.7126\ (sp^{1.00}) + 0.7016\ (sp^{99.99})$ | 0.00 | 0.02 | 99.96 | 99.95 |
| 1.96715 | $\sigma_{C4-C6}$ | −0.62593 | 49.65 | 50.35 | $0.7046\ (sp^{1.90}) + 0.7096\ (sp^{1.89})$ | 34.52 | 34.54 | 65.45 | 65.43 |
| 1.98624 | $\sigma_{C4-N8}$ | −0.69537 | 40.47 | 59.53 | $0.6362\ (sp^{2.54}) + 0.7715\ (sp^{2.06})$ | 28.19 | 32.65 | 71.73 | 67.30 |
| 1.98635 | $\sigma_{C6-N7}$ | −0.72307 | 39.97 | 60.03 | $0.6322\ (sp^{2.52}) + 0.7748\ (sp^{1.86})$ | 28.36 | 34.95 | 71.56 | 65.02 |
| 1.98427 | $\sigma_{N7-C9}$ | −0.67097 | 60.59 | 39.41 | $0.7784\ (sp^{2.07}) + 0.6278\ (sp^{3.47})$ | 32.54 | 22.35 | 67.43 | 77.54 |
| 1.98838 | $\pi_{N8-C10}$ | −0.65598 | 60.39 | 39.61 | $0.7771\ (sp^{2.22}) + 0.6293\ (sp^{3.33})$ | 31.06 | 23.09 | 68.90 | 76.81 |
| 1.97833 | $\sigma_{C9-C11}$ | −0.56685 | 50.76 | 49.24 | $0.7125\ (sp^{2.60}) + 0.7017\ (sp^{2.46})$ | 27.74 | 28.90 | 72.23 | 71.07 |
| 1.99093 | $\sigma_{C11-O12}$ | −0.74608 | 31.51 | 68.49 | $0.5613\ (sp^{4.20}) + 0.8276\ (sp^{2.56})$ | 19.19 | 28.08 | 80.58 | 71.85 |
| 1.98245 | $\pi_{O12-N13}$ | −0.74390 | 59.86 | 40.14 | $0.7737\ (sp^{4.17}) + 0.6335\ (sp^{5.69})$ | 19.31 | 14.93 | 80.57 | 84.87 |
| 1.98449 | $\sigma_{N13-C14}$ | −0.82338 | 58.46 | 41.54 | $0.7646\ (sp^{1.45}) + 0.6445\ (sp^{2.18})$ | 40.82 | 31.39 | 59.12 | 68.53 |
| 1.93371 | $\pi_{N13-C14}$ | −0.29985 | 57.18 | 42.82 | $0.7562\ (sp^{1.00}) + 0.6543\ (sp^{1.00})$ | 0.01 | 0.00 | 99.82 | 99.86 |
| 1.96061 | $\sigma_{C14-C15}$ | −0.60250 | 49.72 | 50.28 | $0.7051\ (sp^{2.00}) + 0.7071\ (sp^{2.19})$ | 33.34 | 31.32 | 66.64 | 68.65 |
| 1.97175 | $\sigma_{C14-C16}$ | −0.60593 | 49.61 | 50.39 | $0.7044\ (sp^{1.84}) + 0.7098\ (sp^{2.25})$ | 35.18 | 30.75 | 64.79 | 69.22 |
| 1.97337 | $\sigma_{C15-C22}$ | −0.63319 | 51.39 | 48.61 | $0.7169\ (sp^{1.92}) + 0.6972\ (sp^{1.92})$ | 34.22 | 34.20 | 65.76 | 65.77 |
| 1.63364 | $\pi_{C15-C22}$ | −0.23406 | 51.47 | 48.53 | $0.7174\ (sp^{1.00}) + 0.6967\ (sp^{1.00})$ | 0.00 | 0.00 | 99.97 | 99.96 |
| 1.97093 | $\sigma_{C16-C17}$ | −0.63744 | 51.30 | 48.70 | $0.7162\ (sp^{1.90}) + 0.6978\ (sp^{1.90})$ | 34.53 | 34.48 | 65.45 | 65.49 |
| 1.65136 | $\pi_{C16-C17}$ | −0.23581 | 51.67 | 48.33 | $0.7188\ (sp^{99.99}) + 0.6952\ (sp^{1.00})$ | 0.01 | 0.01 | 99.96 | 99.96 |
| 1.97976 | $\sigma_{C17-C21}$ | −0.63700 | 50.28 | 49.72 | $0.7091\ (sp^{1.83}) + 0.7051\ (sp^{1.87})$ | 35.38 | 34.84 | 64.59 | 65.13 |
| 1.98128 | $\sigma_{C20-C21}$ | −0.63568 | 49.91 | 50.09 | $0.7065\ (sp^{1.87}) + 0.7078\ (sp^{1.86})$ | 34.85 | 34.96 | 65.12 | 65.01 |
| 1.65328 | $\pi_{C20-C21}$ | −0.23487 | 49.79 | 50.21 | $0.7056\ (sp^{1.00}) + 0.7086\ (sp^{1.00})$ | 0.00 | 0.00 | 99.96 | 99.97 |
| 1.98119 | $\sigma_{C1-H27}$ | −0.45710 | 62.87 | 37.13 | $0.7929\ (sp^{2.32}) + 0.6094\ (s)$ | 30.08 | 100 | 69.88 | – |
| 1.97861 | $\sigma_{C5-H30}$ | −0.45956 | 62.73 | 37.27 | $0.7920\ (sp^{2.36}) + 0.6105\ (s)$ | 29.77 | 100 | 70.19 | – |
| 1.98227 | $\sigma_{N7-H31}$ | −0.57606 | 72.23 | 27.77 | $0.8499\ (sp^{2.81}) + 0.5270\ (s)$ | 26.20 | 100 | 73.75 | – |
| 1.97200 | $\sigma_{N8-H32}$ | −0.55596 | 72.08 | 27.92 | $0.8490\ (sp^{3.11}) + 0.5284\ (s)$ | 24.30 | 100 | 75.65 | – |
| 1.98030 | $\sigma_{C11-H36}$ | −0.46263 | 62.49 | 37.51 | $0.7905\ (sp^{2.29}) + 0.6125\ (s)$ | 25.73 | 100 | 74.12 | – |
| 1.97970 | $\sigma_{C17-H38}$ | −0.47053 | 63.42 | 36.58 | $0.7963\ (sp^{2.29}) + 0.6048\ (s)$ | 30.10 | 100 | 69.86 | – |
| 1.97926 | $\sigma_{C26-H47}$ | −0.46666 | 63.51 | 36.49 | $0.7969\ (sp^{2.29}) + 0.6041\ (s)$ | 30.35 | 100 | 69.61 | – |
| 1.77796 | $n(1)_{N7}$ | −0.22676 | – | – | $sp^{15.12}$ | 6.20 | – | 93.77 | – |
| 1.83556 | $n(1)_{N8}$ | −0.23813 | – | – | $sp^{7.38}$ | 11.93 | – | 88.02 | – |
| 1.97586 | $n(1)_{O1}$ | −0.58497 | – | – | $sp^{0.91}$ | 52.47 | – | 47.50 | – |
| 1.84458 | $n(2)_{O12}$ | −0.27387 | – | – | $sp^{99.99}$ | 0.34 | – | 99.58 | – |
| 1.94695 | $n(1)_{N13}$ | −0.39423 | – | – | $sp^{1.25}$ | 44.43 | – | 55.52 | – |

[a] A-B is the bond between atom A and atom B. (A: natural bond orbital and the polarization coefficient of atom; A-B: natural bond orbital and the polarization coefficient of atom B).

The polarization coefficients C1=0.6973 and C5=0.7168 indicate the importance of the C5 atom in the forming of the $\pi_{C1-C5}$ bonding orbital as opposed to the C1 atom. The $\pi_{C1-C5}$ bonding orbital has the 48.62% and 51.38% C1 and C5 characters, respectively, for the $sp^{1.00}$ hybrids. The sp hybrids of C1 and C5 atoms have 99.96% and 99.97% *p*-characters, respectively. Hence, $\pi\rightarrow\pi^*$ interactions takes place between $\pi_{C1-C5}$ bonding orbital, and $\pi^*_{C4-C6}$ antibonding orbital are stabilized by 14.57 kcal/mol [$\pi_{C1-C5}\rightarrow\pi^*_{C4-C6}$]. The $\pi_{C16-C17}$ bonding orbital in the phenyl ring is determined as $\sigma=0.7188(sp^{99.99})+0.6952(sp^{1.00})$, with an occupancy of 1.65136 a.u. and energy −0.23581 a.u. The polarization coefficients of the C16=0.7188 and

the C17=0.6952 reveal the significance of the C16 atom in forming the $\pi_{C16-C17}$ bond as opposed to the C17 atom.

The $\pi_{C16-C17}$ bonding orbital has a 51.67% C16 character with $sp^{99.99}$ hybrid while the C17 character has 48.33% with $sp^{1.00}$ hybrid. The sp hybrids of these atoms have a $p$-character of 99.96%. Thus, the $\pi_{C16-C17}{\rightarrow}\pi^{*}_{C18-C19}$ interactions takes place between $\pi_{C16-C17}$ bonding orbital and $\pi^{*}_{C18-C19}$ antibonding orbital with a high resonance energy of 14.69 kcal/mol (Table 2). NBO analysis indicates that the lone pair of the N7 atom $[n(1)_{N7}]$ has a $p$-character (93.77%) and high occupancy (1.77796 a.u.) in the studied molecules, leading to stronger stabilization interactions. Thus, the electron donation to the $\pi^{*}_{C4-C6}$ antibonding orbital for the $LP(1)_{N7}{\rightarrow}\pi^{*}_{C4-C6}$ interactions with a high resonance energy of 27.97 kcal/mol (Table 2). The interaction of $LP(2)_{O12}{\rightarrow}\pi^{*}_{N13-C14}$ has higher stabilization energy of 16.10 kcal/mol when it has a $p$-character (99.58%) with occupation number (1.84458 a.u) in molecule **1d**.

### 3.4. Electronic structure and excited states of the compounds 1a−e.

The theoretical absorption spectra of molecules **1a**, **1b**, **1c**, **1d**, and **1e** were determined at the TDPBE1PBE/6-31+G$^{*}$ level in the water. We have computed numbers of excited states using TD-DFT calculations for studied molecules summarized in Tables 4−8. The highest signal in the electronic absorption spectrum of molecule **1a** is detected at $\lambda_{max}$=232 nm with oscillator strength f = 0.23 (Table 4). The charge transfer at $\lambda_{max}$= 232 nm is relevant to the first excited state $S_{o}{\rightarrow}S_{19}$ with seven electron configurations such as H−1→L+6 (3%), H→L+11 (3%), H−2→L+2 (4%), H−1→L+3 (5%), H−1→L+2 (19%), H−1→L+5 (27%), and H−1→L+4 (29%), that the highest transition is from HOMO−1 to LUMO+4. As shown in Table 4, the other excited states of molecule **1a** have a very small intensity and do not play a critical role in forming the electron spectrum. Also, the electronic absorption spectrum of compound **1b** reveals a high signal that belongs to $\lambda_{max}$= 240 nm with f = 0.13 (Table 5). The charge transfer at $\lambda_{max}$= 240 is related to the excited state $S_{o}{\rightarrow}S_{17}$ and is defined by five configurations, including H→L+12 (6%), H−1→L+3 (18%), H−1→L+2 (21%), H−2→L+2 (21%), and H−1→L+4 (27%), that the highest transition is from HOMO−1 to LUMO+4. As can be seen in Table 5, the other excited states of compound **1b** have a very minimal intensity that is almost prohibited by orbital symmetry considerations.

As shown in Table 6, the highest signal in the electronic absorption spectrum of compound **1c** is revealed at $\lambda_{max}$=296 nm with oscillator strength f = 0.44, that the charge transfer is important for the first excited state $S_{o}{\rightarrow}S_{9}$ with two electron configurations, namely H−2→L (88%) and H−2→L+1 (3%) that the main transition is from HOMO−2 to LUMO (H−2→L). The other excited states of molecule **1c** have very small intensities and play little part in forming the electron spectrum.

The theoretical electronic absorption spectrum of **1c** in the solvent water is shown in Figure 5. As can be seen from Table 7, electronic spectra absorption of compound **1d** reveals a strong signal at $\lambda_{max}$= 281 nm with f = 0.23. As can be seen from Table 7, the charge transfer at $\lambda_{max}$= 281 is connected to the $S_{o}{\rightarrow}S_{20}$ excited state. It is described by six configurations, comprising H−5→L+1 (2%), H−2→L (3%), H−6→L (9%), H−7→L (13%), H−2→L+1 (18%), and H−5→L (49%) in which involve significant interaction with the transition from HOMO−5 to the LUMO (H−5→L). The other excited states of compound **1d** have a very small

intensity that is almost restricted by orbital symmetry considerations. The UV spectrum obtained from molecule **1b** in water is seen in Figure 5.

**Table 4.** Electronic absorption spectrum of compound **1a.**

| Excited State | Wavelength (nm) | Excitation Energy (eV) | Configurations Composition (corresponding transition orbitals) | Oscillator Strength (f) |
|---|---|---|---|---|
| $S_0 \to S_1$ | 385 | 3.21 | H→L (100%) | 0.00 |
| $S_0 \to S_2$ | 325 | 3.80 | H→L+1 (88%), H−1→L+2 (7%), H→L+3 (2%) | 0.09 |
| $S_0 \to S_3$ | 315 | 3.93 | H→L+2 (38%), H→L+3 (57%), H→L+4 (2%) | 0.01 |
| $S_0 \to S_4$ | 298 | 4.15 | H→L+2 (22%), H→L+3 (27%), H→L+4 (47%), H→L+5 (2%) | 0.01 |
| $S_0 \to S_5$ | 293 | 4.22 | H−1→L (99%) | 0.00 |
| $S_0 \to S_6$ | 285 | 4.33 | H→L+2 (16%), H→L+4 (40%), H→L+5 (32%), H→L+3 (7%), H→L+6 (3%) | 0.02 |
| $S_0 \to S_7$ | 277 | 4.46 | H→L+5 (56%), H→L+6 (22%), H→L+2 (9%), H→L+3 (3%), H→L+4 (6%), H→L+8 (3%) | 0.02 |
| $S_0 \to S_8$ | 273 | 4.52 | H→L+6 (74%), H→L+2 (6%), H→L+3 (2%), H→L+4 (4%), H→L+5 (8%), H→L+8 (3%) | 0.01 |
| $S_0 \to S_9$ | 264 | 4.69 | H→L+7 (99%) | 0.00 |
| $S_0 \to S_{10}$ | 257 | 4.81 | H−1→L+1 (16%), H→L+8 (68%), H−2→L+1 (8%), H→L+9 (2%) | 0.00 |
| $S_0 \to S_{11}$ | 255 | 4.84 | H−2→L+1 (50%), H−1→L+1 (22%), H→L+8 (18%), H→L+9 (4%) | 0.02 |
| $S_0 \to S_{12}$ | 254 | 4.87 | H→L+9 (94%), H→L+8 (4%) | 0.00 |
| $S_0 \to S_{13}$ | 251 | 4.93 | H−2→L+1 (21%), H−1→L+1 (18%), H−1→L+2 (16%), H−1→L+3 (40%) | 0.04 |
| $S_0 \to S_{14}$ | 247 | 5.01 | H−2→L+1 (18%), H−1→L+1 (30%), H−1→L+2 (11%), H−1→L+3 (27%), H−4→L+1 (2%), H−1→L+4 (5%) | 0.05 |
| $S_0 \to S_{15}$ | 240 | 5.14 | H→L+10 (92%), H−2→L+2 (4%) | 0.00 |
| $S_0 \to S_{16}$ | 239 | 5.17 | H−2→L+2 (24%), H−1→L+2 (20%), H−1→L+3 (17%), H−1→L+4 (28%), H→L+10 (3%) | 0.11 |
| $S_0 \to S_{17}$ | 236 | 5.23 | H−2→L+2 (61%), H−1→L+4 (29%) | 0.01 |
| $S_0 \to S_{18}$ | 234 | 5.28 | H→L+11 (93%), H−2→L+2 (3%) | 0.00 |
| $S_0 \to S_{19}$ | 232 | 5.35 | H−1→L+2 (19%), H−1→L+4 (29%), H−1→L+5 (27%), H−2→L+2 (4%), H−1→L+3 (5%), H−1→L+6 (3%), H→L+11 (3%) | 0.23 |
| $S_0 \to S_{20}$ | 231 | 5.36 | H→L+12 (94%) | 0.00 |

*H-HOMO, L-LUMO

**Table 5.** Electronic absorption spectrum of compound **1b**.

| Excited State | Wavelength (nm) | Excitation Energy (eV) | Configurations Composition (corresponding transition orbitals) | Oscillator Strength (f) |
|---|---|---|---|---|
| $S_0 \to S_1$ | 391 | 3.16 | H→L (100%) | 0.00 |
| $S_0 \to S_2$ | 326 | 3.80 | H→L+1 (87%), H−1→L+2 (7%), H→L+3 (4%) | 0.08 |
| $S_0 \to S_3$ | 315 | 3.92 | H→L+2 (36%), H→L+3 (57%), H→L+1 (3%), H→L+4 (2%) | 0.02 |
| $S_0 \to S_4$ | 299 | 4.14 | H→L+2 (23%), H→L+3 (26%), H→L+4 (45%) | 0.01 |
| $S_0 \to S_5$ | 297 | 4.17 | H−1→L (99%) | 0.00 |
| $S_0 \to S_6$ | 285 | 4.34 | H→L+2 (18%), H→L+4 (41%), H→L+5 (26%), H→L+3 (6%), H→L+6 (5%) | 0.03 |
| $S_0 \to S_7$ | 277 | 4.46 | H→L+5 (37%), H→L+6 (58%) | 0.00 |
| $S_0 \to S_8$ | 275 | 4.50 | H→L+2 (11%), H→L+5 (33%), H→L+6 (36%), H→L+3 (3%), H→L+4 (8%), H→L+8 (5%) | 0.02 |
| $S_0 \to S_9$ | 265 | 4.67 | H→L+7 (97%), H→L+8 (2%) | 0.00 |
| $S_0 \to S_{10}$ | 258 | 4.79 | H→L+8 (81%), H−2→L+1 (2%), H−1→L+1 (8%), H→L+2 (3%) | 0.00 |
| $S_0 \to S_{11}$ | 257 | 4.82 | H−1→L+1 (10%), H→L+9 (79%), H−2→L+1 (8%) | 0.00 |
| $S_0 \to S_{12}$ | 256 | 4.84 | H−2→L+1 (45%), H−1→L+1 (23%), H→L+9 (19%), H−1→L+3 (2%), H→L+8 (6%) | 0.02 |
| $S_0 \to S_{13}$ | 252 | 4.91 | H−2→L+1 (25%), H−1→L+1 (13%), H−1→L+2 (16%), H−1→L+3 (43%) | 0.04 |
| $S_0 \to S_{14}$ | 247 | 5.01 | H−2→L+1 (19%), H−1→L+1 (30%), H−1→L+2 (10%), H−1→L+3 (24%), H−4→L+1 (2%), H−1→L+4 (5%), H→L+10 (3%) | 0.04 |
| $S_0 \to S_{15}$ | 245 | 5.04 | H→L+10 (96%) | 0.00 |
| $S_0 \to S_{16}$ | 242 | 5.11 | H→L+11 (98%) | 0.00 |
| $S_0 \to S_{17}$ | 240 | 5.16 | H−2→L+2 (21%), H−1→L+2 (21%), H−1→L+3 (18%), H−1→L+4 (27%), H→L+12 (6%) | 0.13 |

| Excited State | Wavelength (nm) | Excitation Energy (eV) | Configurations Composition (corresponding transition orbitals) | Oscillator Strength (f) |
|---|---|---|---|---|
| $S_0{\to}S_{18}$ | 237 | 5.21 | H−1→L+4 (19%), H→L+12 (72%), H−2→L+2 (7%) | 0.00 |
| $S_0{\to}S_{19}$ | 236 | 5.23 | H−2→L+2 (64%), H→L+12 (18%), H−1→L+4 (9%), H→L+13 (3%) | 0.03 |
| $S_0{\to}S_{20}$ | 232 | 5.33 | H→L+13 (88%), H−1→L+4 (3%) | 0.02 |

*H-HOMO, L-LUMO

**Table 6.** Electronic absorption spectrum of compound **1c**.

| Excited State | Wavelength (nm) | Excitation Energy (eV) | Configurations Composition (corresponding transition orbitals) | Oscillator Strength (f) |
|---|---|---|---|---|
| $S_0{\to}S_1$ | 574 | 2.15 | H→L (100%) | 0.00 |
| $S_0{\to}S_2$ | 416 | 2.97 | H→L+1 (100%) | 0.00 |
| $S_0{\to}S_3$ | 391 | 3.16 | H−1→L (99%) | 0.00 |
| $S_0{\to}S_4$ | 325 | 3.80 | H→L+2 (87%), H−1→L+3 (6%), H→L+5 (3%) | 0.10 |
| $S_0{\to}S_5$ | 316 | 3.91 | H→L+3 (32%), H→L+4 (59%), H→L+5 (4%) | 0.01 |
| $S_0{\to}S_6$ | 311 | 3.98 | H→L+4 (15%), H→L+5 (75%), H−1→L+1 (6%), H→L+3 (3%) | 0.00 |
| $S_0{\to}S_7$ | 310 | 3.99 | H−1→L+1 (94%)   H→L+5 (5%), | 0.00 |
| $S_0{\to}S_8$ | 299 | 4.13 | H→L+3 (25%), H→L+4 (15%), H→L+5 (10%), H→L+6 (44%), H→L+7 (3%) | 0.01 |
| $S_0{\to}S_9$ | 296 | 4.18 | H−2→L (88%), H−2→L+1 (3%) | 0.44 |
| $S_0{\to}S_{10}$ | 288 | 4.29 | H→L+6 (27%), H→L+7 (64%), H→L+3 (5%) | 0.00 |
| $S_0{\to}S_{11}$ | 286 | 4.33 | H−3→L (38%), H−2→L+1 (57%), H−2→L (3%) | 0.02 |
| $S_0{\to}S_{12}$ | 281 | 4.39 | H→L+3 (18%), H→L+6 (20%), H→L+7 (29%), H→L+8 (19%), H→L+4 (4%), H→L+9 (2%) | 0.03 |
| $S_0{\to}S_{13}$ | 274 | 4.52 | H→L+8 (75%), H→L+3 (6%), H→L+6 (4%), H→L+9 (7%) | 0.01 |
| $S_0{\to}S_{14}$ | 268 | 4.61 | H→L+9 (87%), H→L+3 (2%), H→L+8 (2%), H→L+10 (2%), H→L+11 (2%) | 0.01 |
| $S_0{\to}S_{15}$ | 266 | 4.65 | H−4→L (69%), H−3→L (20%), H−2→L+1 (7%) | 0.01 |
| $S_0{\to}S_{16}$ | 264 | 4.68 | H−2→L+2 (87%), H−1→L+2 (10%) | 0.00 |
| $S_0{\to}S_{17}$ | 263 | 4.70 | H→L+10 (93%), H→L+11 (3%) | 0.00 |
| $S_0{\to}S_{18}$ | 258 | 4.80 | H−4→L (21%), H−3→L (27%), H−2→L+1 (22%), H→L+11 (14%), H−5→L+1 (8%) | 0.05 |
| $S_0{\to}S_{19}$ | 257 | 4.81 | H−4→L (4%), H−3→L (5%), H→L+11(75%),H−2→L+1(4%) | 0.00 |
| $S_0{\to}S_{20}$ | 253 | 4.89 | H−1→L+2 (33%), H−1→L+4 (21%), H−1→L+5 (13%), H→L+12 (16%), H−2→L+2 (4%), H−1→L+3 (9%) | 0.02 |

*H-HOMO, L-LUMO

**Table 7.** Electronic absorption spectrum of compound **1d.**

| Excited State | Wavelength (nm) | Excitation Energy (eV) | Configurations Composition (corresponding transition orbitals) | Oscillator Strength (f) |
|---|---|---|---|---|
| $S_0{\to}S_1$ | 608 | 2.03 | H→L (100%) | 0.00 |
| $S_0{\to}S_2$ | 435 | 2.84 | H→L+1 (99%) | 0.00 |
| $S_0{\to}S_3$ | 431 | 2.87 | H−1→L (100%) | 0.00 |
| $S_0{\to}S_4$ | 429 | 2.88 | H→L+2 (99%) | 0.00 |
| $S_0{\to}S_5$ | 386 | 3.20 | H→L+3 (100%) | 0.00 |
| $S_0{\to}S_6$ | 336 | 3.68 | H−1→L+1 (99%) | 0.00 |
| $S_0{\to}S_7$ | 332 | 3.72 | H−1→L+2 (94%),H-2→L (5%) | 0.01 |
| $S_0{\to}S_8$ | 332 | 3.73 | H−2→L (70%), H→L+4 (11%), H−2→L+1 (8%), H−1→L+2 (6%) | 0.13 |
| $S_0{\to}S_9$ | 325 | 3.80 | H→L+4 (67%), H−2→L (9%), H−1→L+5 (3%), H→L+5 (7%), H→L+6 (9%) | 0.08 |
| $S_0{\to}S_{10}$ | 315 | 3.93 | H→L+4 (12%), H→L+5 (40%), H→L+6 (44%) | 0.01 |
| $S_0{\to}S_{11}$ | 306 | 4.04 | H−1→L+3 (99%) | 0.00 |
| $S_0{\to}S_{12}$ | 305 | 4.05 | H−5→L (13%), H−4→L (15%), H−2→L+1 (25%), H−2→L+2 (41%), H−3→L (3%), H−2→L (2%) | 0.02 |
| $S_0{\to}S_{13}$ | 304 | 4.06 | H−2→L+1 (35%), H−2→L+2 (42%), H−6→L (4%), H−5→L (9%), H−3→L (6%), H−2→L (2%) | 0.01 |
| $S_0{\to}S_{14}$ | 299 | 4.14 | H−4→L (31%), H−3→L (51%), H−2→L+1 (2%), H−2→L+3 (8%) | 0.01 |
| $S_0{\to}S_{15}$ | 294 | 4.21 | H−5→L (12%), H−4→L (39%), H−3→L (20%), H−7→L (6%), H−6→L (5%), H−2→L+2 (6%), H−2→L+3 (6%) | 0.00 |
| $S_0{\to}S_{16}$ | 293 | 4.22 | H→L+7 (94%), H→L+5 (2%), H→L+6 (2%) | 0.00 |
| $S_0{\to}S_{17}$ | 289 | 4.28 | H→L+8 (96%) | 0.00 |
| $S_0{\to}S_{18}$ | 287 | 4.31 | H−6→L (66%), H−7→L (4%), H−5→L (9%), H−4→L (4%), H−3→L+1 (2%), H−2→L+2 (4%), H−2→L+3 (6%) | 0.01 |

| Excited State | Wavelength (nm) | Excitation Energy (eV) | Configurations Composition (corresponding transition orbitals) | Oscillator Strength (f) |
|---|---|---|---|---|
| $S_0 \rightarrow S_{19}$ | 285 | 4.33 | H→L+9 (79%), H→L+5 (8%), H→L+6 (8%), H→L+7 (2%) | 0.00 |
| $S_0 \rightarrow S_{20}$ | 281 | 4.40 | H−7→L (13%), H−5→L (49%), H−2→L+1 (18%), H−6→L (9%), H−5→L+1 (2%), H−2→L (3%) | 0.23 |

*H-HOMO, L-LUMO

**Table 8.** Electronic absorption spectrum of compound **1e**.

| Excited State | Wavelength (nm) | Excitation Energy (eV) | Configurations Composition (corresponding transition orbitals) | Oscillator Strength (f) |
|---|---|---|---|---|
| $S_0 \rightarrow S_1$ | 895 | 1.38 | H→L (100%) | 0.01 |
| $S_0 \rightarrow S_2$ | 530 | 2.33 | H→L+1 (100%) | 0.00 |
| $S_0 \rightarrow S_3$ | 520 | 2.38 | H−1→L (100%) | 0.00 |
| $S_0 \rightarrow S_4$ | 426 | 2.90 | H−2→L (90%), H−3→L (8%) | 0.00 |
| $S_0 \rightarrow S_5$ | 391 | 3.16 | H→L+2 (100%) | 0.00 |
| $S_0 \rightarrow S_6$ | 371 | 3.33 | H−1→L+1 (100%) | 0.00 |
| $S_0 \rightarrow S_7$ | 353 | 3.50 | H−4→L (12%), H−3→L (70%), H−2→L (7%), H−2→L+1 (4%) | 0.28 |
| $S_0 \rightarrow S_8$ | 330 | 3.75 | H−4→L (67%), H−3→L (10%), H−2→L+1 (10%), H−3→L+1 (6%), HO→L+3 (3%) | 0.09 |
| $S_0 \rightarrow S_9$ | 323 | 3.83 | H→L+3 (85%), H−3→L+1 (2%), H−1→L+4 (7%) | 0.08 |
| $S_0 \rightarrow S_{10}$ | 315 | 3.92 | H−3→L+1 (67%), H−2→L+1 (20%), H−3→L (5%) | 0.02 |
| $S_0 \rightarrow S_{11}$ | 314 | 3.94 | H→L+5 (98%) | 0.00 |
| $S_0 \rightarrow S_{12}$ | 313 | 3.95 | H→L+4 (41%), H→L+6 (54%), H→L+7 (3%) | 0.01 |
| $S_0 \rightarrow S_{13}$ | 309 | 4.00 | H−5→L (96%) | 0.00 |
| $S_0 \rightarrow S_{14}$ | 298 | 4.16 | H−7→L (86%), H→L+4 (3%), H→L+6 (4%), H→L+7 (6%) | 0.00 |
| $S_0 \rightarrow S_{15}$ | 297 | 4.17 | H−1→L+2 (99%) | 0.00 |
| $S_0 \rightarrow S_{16}$ | 297 | 4.17 | H−7→L (12%), H→L+4 (16%), H→L+6 (25%), H→L+7 (44%) | 0.00 |
| $S_0 \rightarrow S_{17}$ | 293 | 4.22 | H−8→L (28%), H−6→L (60%), H−5→L (3%), H−2→L+1 (3%) | 0.01 |
| $S_0 \rightarrow S_{18}$ | 288 | 4.29 | H→L+8 (99%) | 0.00 |
| $S_0 \rightarrow S_{19}$ | 286 | 4.32 | H-4→L (11%), H-3→L+1 (14%), H-3→L+2 (16%), H-2→L+1 (46%), H-8→L (3%), H-4→L+1 (3%), H-2→L+2 (2%) | 0.38 |
| $S_0 \rightarrow S_{20}$ | 282 | 4.39 | H→L+4 (20%), H→L+7 (36%), H→L+9 (21%), H→L+6 (9%), H→L+10 (9%) | 0.04 |

*H-HOMO, L-LUMO

As shown in Table 5, the highest absorption in $\lambda_{max}$= 286 nm with oscillator strength f=0.38 for molecule 1e is connected to the first excited state of $S_o \rightarrow S_{19}$ with seven electron configurations, namely, H−2→L+2 (2%), H−8→L (3%), H−4→L+1 (3%), H−4→L (11%), H−3→L+1 (14%), H−3→L+2 (16%), and H−2→L+1 (46%) that the main transition is from the HOMO−2 to the LUMO+1 (H−2→L+1). The 7th excited state is also deserving of attention: $S_o \rightarrow S_7$ at $\lambda_{max}$= 353 nm with oscillator strength f=0.28 and four configurations for electronic excitations including H−2→L+1 (4%), H−2→L (7%), H−4→L (12%), and H−3→L (70%).

The other excited states of molecule 1e do not have a key role in the formation of the electron spectrum and have a very small intensity. The theoretical electronic absorption spectrum of molecule 1e in solvent water is seen in Figure 5.

## 4. Conclusions

The design of new oxime ether derivatives containing a quinoxaline moiety was investigated using the DFT/PBE1PBE/6-31+G$^*$ theoretical level. The calculated results showed that the highest global hardness value is observed for molecule **1a** (R1=R2=CH$_3$). According to NBO analysis of compound **1d**, (R1=R2=Ph), the π-bonds and lone pairs with p-character participate in the electron donation to π$^*$-bonds that lead to high stabilization energy. The global hardness values of molecules **1a**, **1b**, **1c**, **1d**, and **1e** are 1.60, 1.57, 1.08, 1.01 and 0.69 eV, respectively.
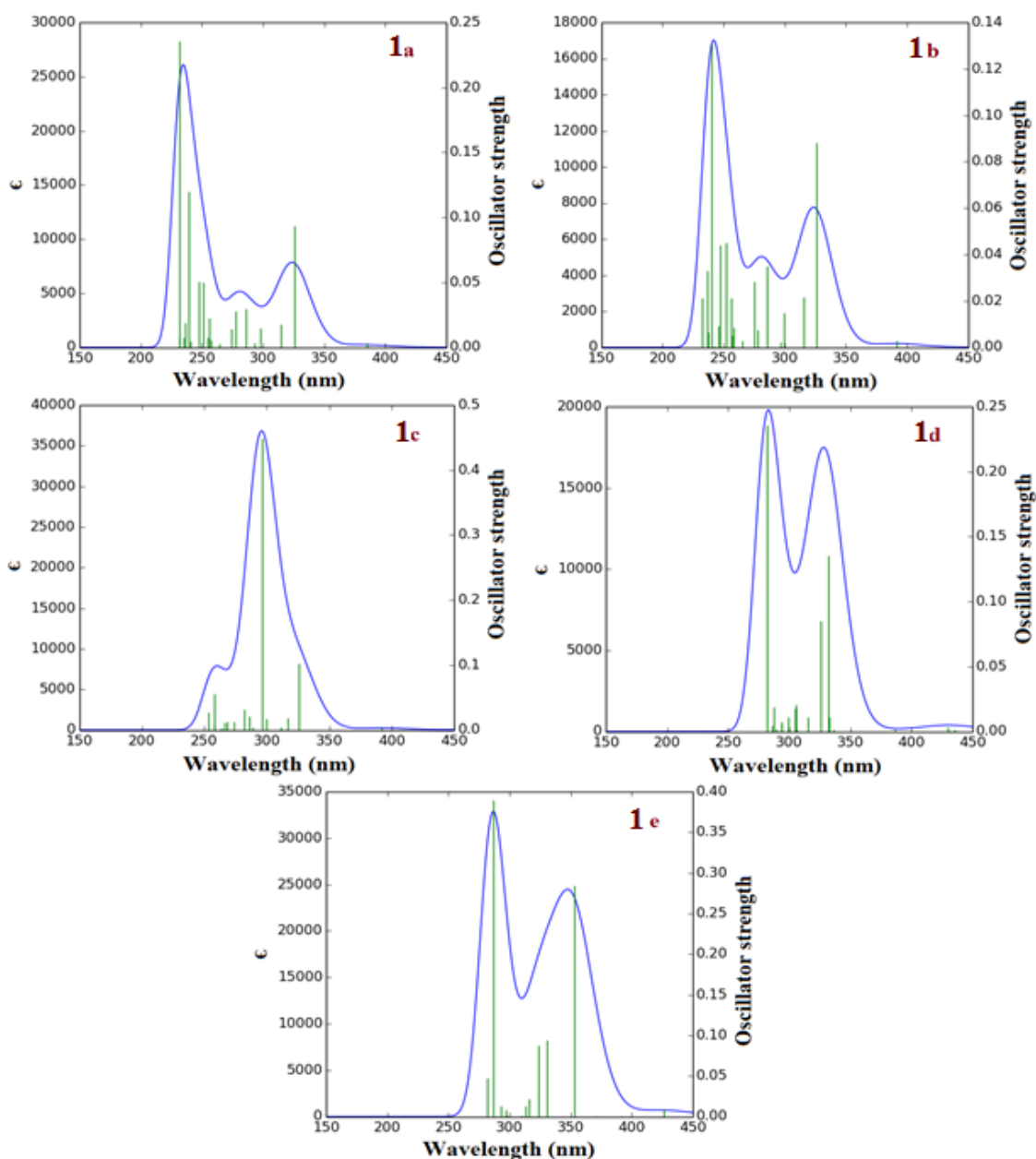
**Figure 5**. The theoretical UV spectra of compounds **1a−e** in the solvent.

The highest global hardness value is observed for molecule 1a; thus, it is the hardest molecule compared to other molecules. The strongest signals in electronic absorption spectra of the molecules **1a**, **1b**, **1c**, **1d**, and **1e** are observed at $\lambda_{max} = 232$, 240, 296, 281, and 286 nm.

## Funding

## Acknowledgments

## Conflicts of Interest

The authors declare no conflict of interest.

## References

1.  Matada, B.S.; Pattanashettar R.; Yernale N.G. A comprehensive review on the biological interest of quinoline and its derivatives. *Bioorg. Med. Chem.* **2021**, *32*, 115973, https://doi.org/10.1016/j.bmc.2020.115973.

2.  Merdas S.M.; Hayal M.Y. Heterocyclic Compounds Containing N atoms as Corrosion Inhibitors: A review. *Journal of Bioscience and Applied Research* **2021**, *7,* 93-103, https://doi.org/10.21608/jbaar.2021.178505.

3.  Shukla, P.K.; Verma, A.; Mishra, P. Significance of nitrogen heterocyclic nuclei in the search of pharmacological active compounds. New Perspective in Agricultural and Human Health; Shukla, RP, Mishra, RS, Tripathi, AD, Yadav, AK, Tiwari, M, Mishra, RR, Eds. **2017**, 100-26.

4.  Montana, M.; Montero. V.; Khoumeri. O.; Vanelle P. Quinoxaline Moiety: A Potential Scaffold against Mycobacterium tuberculosis. *Molecules* **2021**, *26,* 4742, https://doi.org/10.3390/molecules26164742.

5.  Irfan, A.; Sabeeh. I.; Umer. M.; Naqvi A.Z.; Fatima H.; Yousaf S. A review on the Terapeutic Potential of Quinoxaline Derivatives. *World Journal of Pharmaceutical Research* **2017**, *6*, https://doi.org/10.20959/wjpr201713-9878.

6.  Zarenezhad, E.; Mosslemin, M.H.; Alborzi. A.; Anaraki-Ardakani .H.; Shams N.; Khoshnood, M.M. Efficient Synthesis of 3, 4-Dihydro-1 H-Quinoxalin-2-ones and 1 H-Quinolin-2-Ones and Evaluation of Their Antibacterial Activity. *Journal of Chemical Research* **2014**, *38,* 337-40, https://doi.org/10.3184/174751914X13987604216112.

7.  Vázquez-Lizardi, G.A.; Ruiz-Casanova, L.A.; Cruz-Sánchez, R.M.; Santana, J.A. Simulation of metal-supported metal-Nanoislands: A comparison of DFT methods. *Surface Science* **2021**, *712*, 121889, https://doi.org/10.1016/j.susc.2021.121889.

8.  Gi,l A.; Pabón, A.; Galiano. S; Burguete. A.; Pérez-Silanes, S.; Deharo, E. Synthesis, biological evaluation and structure-activity relationships of new quinoxaline derivatives as anti-Plasmodium falciparum agents. *Molecules* **2014**, *19,* 2166-80, https://doi.org/10.3390/molecules19022166.

9.  El-Helby, A.GA.; Ayyad R.R.; El-Adl K.; Sakr H.; Abd-Elrahman A.A.; Eissa I.H.; Elwan A. Design, molecular docking and synthesis of some novel 4-acetyl-1-substituted-3, 4-dihydroquinoxalin-2 (1H)-one derivatives for anticonvulsant evaluation as AMPA-receptor antagonists. *Medicinal Chemistry Research* **2016**, *25,* 3030-46, https://doi.org/10.1007/s00044-016-1723-7.

10. Piras, S.; Loriga, M.; Paglietti, G. Quinoxaline chemistry. Part XVII. Methyl [4-(substituted 2-quinoxalinyloxy) phenyl] acetates and ethyl N-{[4-(substituted 2-quinoxalinyloxy) phenyl] acetyl} glutamates analogs of methotrexate: synthesis and evaluation of in vitro anticancer activity. *Il farmaco.* **2004,** *59,* 185-94, https://doi.org/10.1016/j.farmac.2003.11.014.

11. Porter. J.; Lumb. S.; Lecomte. F.; Reuberson. J.; Foley, A. Calmiano M.; le Riche, K.; Edwards, H.; Delgado, J.; Franklin, R.L.; Gascon-Simorte, J.M.; Maloney, A.; Meier, C.; Batchelor, M. Discovery of a novel series of quinoxalines as inhibitors of c-Met kinase. *Bioorganic & medicinal chemistry letters* **2009,** *19,* 397-400, https://doi.org/10.1016/j.bmcl.2008.11.062.

12. Behzadi H.; Roonasi P.; van der Spoel D.; Manzetti S. Relationship between electronic properties and drug activity of seven quinoxaline compounds: A DFT study. *Journal of Molecular Structure* **2015**, *1091*, 196-202, https://doi.org/10.1016/j.molstruc.2015.03.001.

13. Abbas H-AS.; Al-Marhabi A.R.; Eissa, S.I.; Ammar, Y.A. Molecular modeling studies and synthesis of novel quinoxaline derivatives with potential anticancer activity as inhibitors of c-Met kinase. *Bioorganic & medicinal chemistry* **2015**, *23*, 6560-72, https://doi.org/10.1016/j.bmc.2015.09.023.

14. Corona, P.; Carta, A.; Loriga. M.; Vitale, G.; Paglietti, G. Synthesis and in vitro antitumor activity of new quinoxaline derivatives. *European journal of medicinal chemistry* **2009**, *44,* 1579-91, https://doi.org/10.1016/j.ejmech.2008.07.025.

15. Zarenezhad, E.; Rad M.N.S.; Mosslemin, M.H.; Tabatabaee, M.; Behrouz, S. Nano-MoO$_3$ as a highly efficient heterogeneous catalyst for a one-pot synthesis of tetrahydropyrimidine derivatives in water. *Journal of Chemical Research* **2014**, *38,* 607-10, https://doi.org/10.3184/174751914X14115772243815.

16. Afsarian, M.H.; Farjam, M.; Zarenezhad, E.; Behrouz, S.; Rad M.N.S. Synthesis, Antifungal Evaluation and Molecular Docking Studies of Some Tetrazole Derivatives. *Acta Chimica Slovenica* **2019**, *66,* 874-87, https://doi.org/10.17344/acsi.2019.4992.

17. Zarenezhad, E.; Farjam, M.; Iraji, A. Synthesis and biological activity of pyrimidines-containing hybrids: Focusing on pharmacological application. *Journal of Molecular Structure*, **2021**, *1230*, 129833, https://doi.org/10.1016/j.molstruc.2020.129833.

18. Frisch M.J.; Trucks G.W.; Schlegel H.B.; Scuseria G.E.; Robb M.A.; Cheeseman J.R.; et al. Gaussian 09. Revision A.02 ed. Wallingford CT,: Gaussian, Inc.; 2009.

19. Maldonado, A.M.; Hagiwara, S.; Choi, T.H.; Eckert, F.; Schwarz. K.; Sundararaman, R. Quantifying uncertainties in solvation procedures for modeling aqueous phase reaction mechanisms. *The Journal of Physical Chemistry A* **2021**, *125(1),* 154-64, https://doi.org/10.1021/acs.jpca.0c08961.

20. Farahipour, R. Integration of Quantum Chemistry (QC) Within Computer-Aided Ionic Liquid Design (CAILD) Framework (Doctoral dissertation, University of Colorado at Denver) **2021.**

21. Frisch, A.; Nielson, A.; Holder, A. Gaussview user manual. Gaussian Inc, Pittsburgh, PA **2000**, 556.

22. Weinhold, F.; Landis, C.R; Natural bond orbitals and extensions of localized bonding concepts. *Chemistry Education Research and Practice* **2001**, *2(2),* 91-104, https://doi.org/10.1039/B1RP90011K.

23. Shahab, S.; Sheikhi, M.; Kvasyuk, E.; Sysa, A.G., Alnajjar, R.; Strogova, A.; Sirotsina, K.; Yurlevich.; H. Novik, D. Geometry Optimization, UV/Vis, NBO, HOMO and LUMO, Excited State and Antioxidant Evaluation of Pyrimidine Derivatives. *Letters in Organic Chemistry* **2021**, *18,* 465-476, https://doi.org/10.2174/1570178617999200812133402.

24. Janani, S.; Rajagopal, H.; Muthu, S.; Aayisha, S.; Raja, M. Molecular structure, spectroscopic (FT-IR, FT-Raman, NMR), HOMO-LUMO, chemical reactivity, AIM, ELF, LOL and Molecular docking studies on 1-Benzyl-4-(N-Boc-amino) piperidine. *Journal of Molecular Structure* **2021**, *1230*, 129657, https://doi.org/10.1016/j.molstruc.2020.129657.

25. Dotsenko, V.V.; Bespalov, A.V.; Vashurin, A.S.; Aksenov, N.A.; Aksenova, I.V.; Chigorina, E.A; Krivokolysko, S.G. 2-Amino-4, 5-dihydrothiophene-3-carbonitriles: A New Synthesis, Quantum Chemical Studies, and Mannich-Type Reactions Leading to New Hexahydrothieno [2, 3-d] pyrimidines. *ACS Omega* **2021**, *6,* 32571-32588, https://pubs.acs.org/doi/10.1021/acsomega.1c04141.

26. Shahab, S.; Sheikhi, M.; Filippovich, L.; Khaleghian, M.; Dikusar, E.; Yahyaei, H. Spectroscopic Studies (Geometry Optimization, E→ Z Isomerization, UV/Vis, Excited States, FT-IR, HOMO-LUMO, FMO, MEP, NBO, Polarization) and Anisotropy of Thermal and Electrical Conductivity of New Azomethine Dyes in Stretched Polymer Matrix. *Silicon* **2018**, *10,* 2361-85, https://doi.org/10.1007/s12633-018-9773-8.

27. Sheikhi, M.; Shahab, S.; Khaleghian.; M, Hajikolaee.; F.H, Balakhanava.; I, Alnajjar R. Adsorption properties of the molecule resveratrol on CNT (8, 0-10) nanotube: Geometry optimization, molecular structure, spectroscopic (NMR, UV/Vis, excited state), FMO, MEP and HOMO-LUMO investigations. *Journal of Molecular Structure* **2018**, *1160*, 479-87, https://doi.org/10.1016/j.molstruc.2018.01.005.

28. Hu, C.; Chen, F.; Wang, Y.; Tian, N.; Ma, T.; Zhang, Y.; Huang, H. Exceptional cocatalyst-free photo-enhanced piezocatalytic hydrogen evolution of carbon nitride nanosheets from strong in-plane polarization. *Advanced Materials* **2021**, *33,* 2101751, https://doi.org/10.1002/adma.202101751.

29. Mohammadi, M.D.; Abdullah, H.Y.; Biskos, G.; Bhowmick, S. Enhancing the absorption of 1-chloro-1, 2, 2, 2-tetrafluoroethane on carbon nanotubes: an ab initio study. *Bulletin of Materials Science* **2021**, *44,* 1-11, https://doi.org/ 10.1007/s12034-021-02472-9.

30. Glendening, E.D.; Landis, C.R.; Weinhold, F. 6 Natural bond orbital theory: Discovering chemistry with NBO7. *Complementary Bonding Analysis* **2021**, 129-156, https://doi.org/10.1515/9783110660074-006.

31. Brand, M.; Ahmadzadeh. K.; Li, X.; Rinkevicius, Z.; Saidi, W.A; Norman, P. Size-dependent polarizabilities and van der Waals dispersion coefficients of fullerenes from large-scale complex polarization propagator calculations. *The Journal of Chemical Physics* **2021**, *154,* 074304, https://doi.org/10.1063/5.0040009.

32. Shinde, R.S. Ultrasound assisted synthesis, molecular structure, UV-visible assignments, MEP and Mulliken charges study of (E)-3-(4-chlorophenyl)-1-(4-methoxyphenyl) prop-2-en-1-one: experimental and DFT correlational. *Material Science Research India* **2021**, *18,* 86-96, http://dx.doi.org/10.13005/msri/180110.